

# Probing the IGM-galaxy connection at $z < 0.5$ II. New insights into the galaxy environments of O VI absorbers in PKS 0405–123

Sean D. Johnson<sup>1\*</sup>, Hsiao-Wen Chen<sup>1†</sup>, John S. Mulchaey<sup>2</sup>

<sup>1</sup>*Department of Astronomy & Astrophysics and Kavli Institute for Cosmological Physics, The University of Chicago, Chicago, IL 60637, USA*

<sup>2</sup>*The Observatories of the Carnegie Institute of Washington, 813 Santa Barbara Street, Pasadena, CA 91101, USA*

17 November 2018

## ABSTRACT

We present new absorption-line analysis and new galaxy survey data obtained for the field around PKS 0405–123 at  $z_{\text{QSO}} = 0.57$ . Combining previously known O VI absorbers with new identifications in the higher  $S/N$  UV spectra obtained with the Cosmic Origins Spectrograph, we have established a sample of seven O VI absorbers and 12 individual components at  $z = 0.0918 - 0.495$  along the sightline toward PKS 0405–123. We complement the available UV absorption spectra with galaxy survey data that reach 100% completeness at projected distances  $\rho < 200$  kpc of the quasar sightline for galaxies as faint as  $0.1 L_*$  ( $0.2 L_*$ ) out to redshifts of  $z \approx 0.35$  ( $z \approx 0.5$ ). The high level of completeness achieved at faint magnitudes by our survey reveals that O VI absorbers are closely associated with gas-rich environments containing at least one low-mass, emission-line galaxy. An intriguing exception is a strong O VI system at  $z \approx 0.183$  that does not have a galaxy found at  $\rho < 4$  Mpc, and our survey rules out the presence of any galaxies of  $L > 0.04 L_*$  at  $\rho < 250$  kpc and any galaxies of  $L > 0.3 L_*$  at  $\rho < 1$  Mpc. We further examine the galactic environments of O VI absorbers and those “Ly $\alpha$ -only” absorbers with neutral hydrogen column density  $\log N(\text{HI}) > 13.6$  and no detectable O VI absorption features. The Ly $\alpha$ -only absorbers serve as a control sample in seeking the discriminating galactic features that result in the observed O VI absorbing gas at large galactic radii. We find a clear distinction in the radial profiles of mean galaxy surface brightness around different absorbers. Specifically, O VI absorbers are found to reside in regions of higher mean surface brightness at  $\rho \lesssim 500$  kpc ( $\Delta\mu_R \approx +5$  mag Mpc<sup>−2</sup> relative to the background at  $\rho > 500$  kpc), while only a mild increase in galaxy surface brightness is seen at small  $\rho$  around Ly $\alpha$ -only absorbers ( $\Delta\mu_R \approx +2$  mag Mpc<sup>−2</sup>). The additional insights gained from our deep galaxy survey demonstrates the need to probe the galaxy populations to low luminosities in order to better understand the nature of the absorbing systems.

**Key words:** surveys – galaxies: haloes – quasars: absorption lines – galaxies: star formation

## 1 INTRODUCTION

Ultraviolet absorption lines in the spectra of background sources represent the most sensitive available means of observing the diffuse gas that permeates the universe. The O VI  $\lambda\lambda 1031, 1037$  doublet in particular has received attention as a tracer of: the warm-hot phase of the intergalactic medium (IGM; e.g. Cen & Ostriker 1999), the galaxy outflows thought to be responsible for the chemical enrichment

of the IGM (e.g. Oppenheimer & Davé 2006), and the intra-group medium (Mulchaey et al. 1996). While independent surveys of O VI absorbers in the spectra of distant quasars have uncovered a large number of these systems supporting the notion of O VI doublets being a sensitive tracer of warm-hot gas, the reported number density of O VI absorbers from different surveys shows a scatter much beyond the individual measurement errors (e.g. Burles & Tytler 1996; Tripp et al. 2000; Tripp & Savage 2000; Prochaska et al. 2004; Richter et al. 2004; Tripp et al. 2008; Thom & Chen 2008; Danforth & Shull 2008; Tilton et al. 2012). At the same time, cosmo-

\* E-mail: seanjohnson@uchicago.edu

† E-mail: hchen@oddjob.uchicago.edu

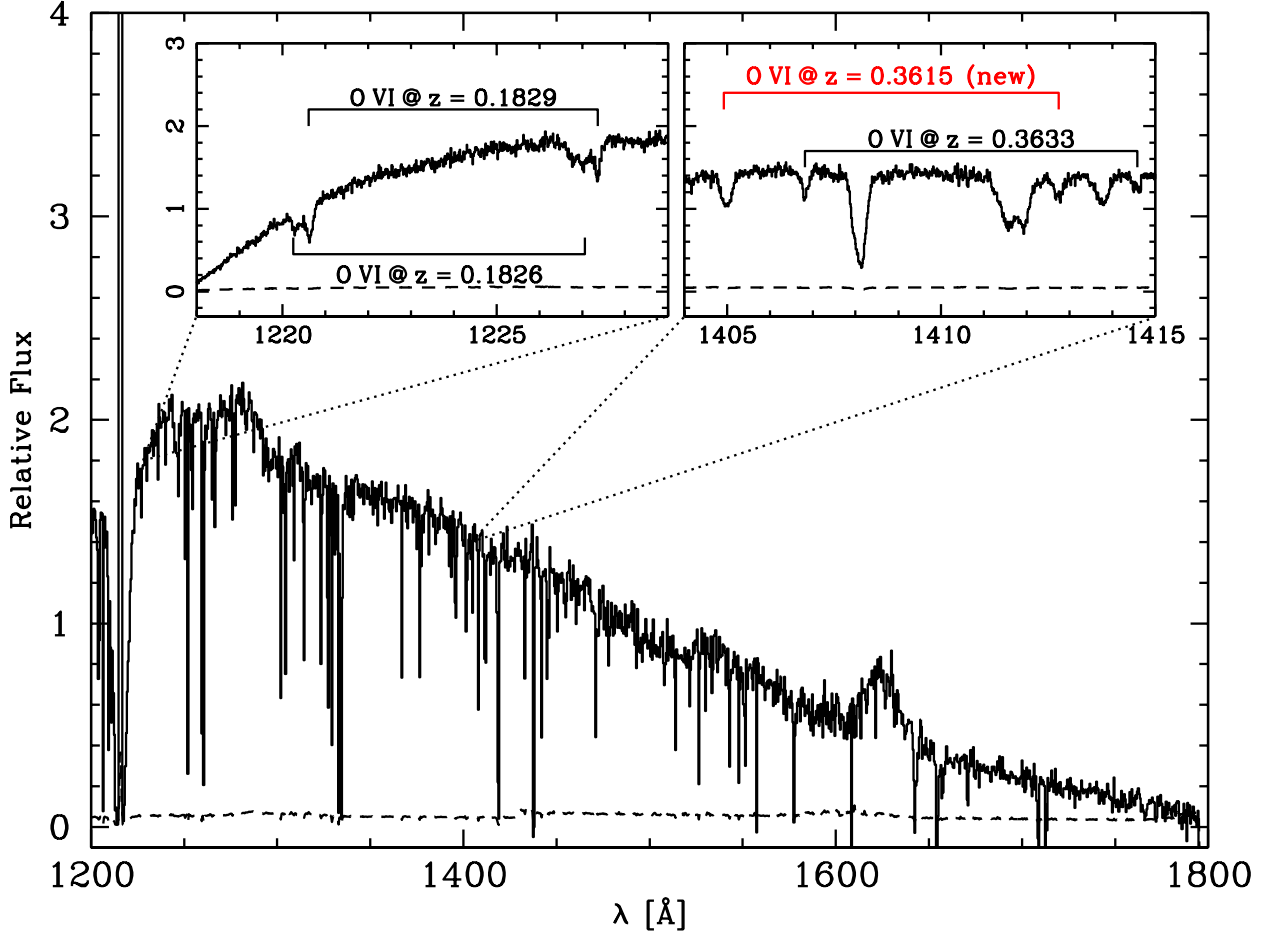


**Figure 1.** Reduced and combined COS spectrum (solid line) of PKS 0405–123 with corresponding  $1\text{-}\sigma$  errors (dashed line). The inset plots highlight detections enabled by the improved  $S/N$  of the quasar spectrum. *Left:* O VI absorption at  $z = 0.1829$  and  $0.1826$ . *Right:* O VI absorption at  $z = 0.3633$  and  $0.3615$  (new).

logical simulations incorporating momentum-driven winds have been able to reproduce the observed O VI absorption column density distribution function, but ambiguity remains in attributing the majority of low-redshift O VI absorbers to either cool, photoionized gas (e.g. Kang et al. 2005; Oppenheimer & Davé 2009; Oppenheimer et al. 2012) or the warm-hot phase of the IGM (cf. Smith et al. 2011; Tepper-García et al. 2011; Cen 2012; Stinson et al. 2012).

Key insights into the physical origin of O VI absorbers can be gained from a detailed examination of their galactic environments. Observations designed to constrain the properties of gaseous halos of known galaxies have shown that emission-line galaxies exhibit near unity O VI covering fractions ( $\kappa_{\text{O VI}}$ ) at projected distances  $\rho \lesssim 150$  kpc and  $\kappa_{\text{O VI}} \approx 64\%$  at  $\rho < 350$  kpc, while absorption-line galaxies exhibit  $\kappa_{\text{O VI}} \lesssim 30\%$  on similar scales (Chen & Mulchaey 2009; Tumlinson et al. 2011). The large incidence of O VI absorbers around star-forming galaxies may be explained by a causal connection between star formation and the production of O VI absorbing gas, but the non-negligible covering fraction of such gas around an evolved galaxy population becomes difficult to explain under the same scenario.

While surveys of galaxies associated with known O VI absorbers have revealed a correlation between the pres-

ence of star-forming galaxies and O VI absorbers at modest projected separations  $\rho \lesssim 350$  kpc (Stocke et al. 2006; Prochaska et al. 2006; Chen & Mulchaey 2009; Mulchaey & Chen 2009; Wakker & Savage 2009; Stocke et al. 2013), the galaxy survey data are not sufficiently deep and complete for a detailed examination of the galactic environment immediate to the absorbers. Dedicated surveys around UV bright quasar sightlines are typically limited to bright galaxies with  $R$ -band magnitudes brighter than  $AB(R) \approx 19.5$  limiting sensitivity to  $L \approx 0.1 L_*$  galaxies at  $z \lesssim 0.1$  (e.g. Prochaska et al. 2011). Although the study of Wakker & Savage (2009) includes galaxies fainter than  $L = 0.1 L_*$  at  $z < 0.02$ , the incompleteness of their galaxy catalog is unknown. Survey incompleteness complicates the interpretation of the galaxy-absorber studies (Stocke et al. 2006, 2013). To date, a high completeness level ( $> 95\%$ ) for galaxies of  $R \lesssim 23$  and  $\Delta\theta \lesssim 2'$  from the quasar sightline has been reached in only one quasar field (HE 0226–4110 in Chen & Mulchaey 2009). To improve the statistics, our group is continuing the effort to collect high-completeness galaxy survey data in multiple quasar fields.

In this paper, we present new galaxy survey data obtained for the field around PKS 0405–123 at  $z_{\text{QSO}} = 0.57$ . Our galaxy survey in this field has reached 100% complete-

ness within  $\rho = 200$  kpc of the quasar sightline for galaxies as faint as  $0.1 L_*$  ( $0.2 L_*$ ) out to redshifts of  $z \approx 0.35$  ( $z \approx 0.5$ ). PKS 0405–123 is among the brightest quasars on the sky, for which high-quality UV echelle data have been obtained using the Space Telescope Imaging Spectrograph (STIS; Woodgate, B. E., et al. 1998) and extremely high-quality UV spectra have been obtained using the new Cosmic Origins Spectrograph (COS; Green et al. 2012) on board the *Hubble Space Telescope* (HST). The intermediate redshift of the quasar provides a long redshift path length for probing intervening absorption systems. Previous systematic searches in the STIS and Far Ultraviolet Spectroscopic Explorer (FUSE; Moos et al. 2000) spectra have uncovered six O VI absorption systems at  $z_{\text{O VI}} = 0.09 - 0.5$  (Prochaska et al. 2004; Howk et al. 2009) and 11 additional strong Ly $\alpha$  absorbers of neutral hydrogen column density  $\log N(\text{H I}) \geq 13.6$  at  $z_{\text{H I}} = 0.03 - 0.5$  (e.g. Williger et al. 2006; Lehner et al. 2007). Recent targeted searches in the new COS spectra have further uncovered a Ne VIII absorber associated with the strong O VI absorber at  $z = 0.495$  (Narayanan et al. 2011) and a new component associated with the previously known O VI absorber at  $z = 0.167$  (Savage et al. 2010).

To complement the available highly complete galaxy survey data, we have carried out a new systematic search of absorption features in the new COS spectra. Here we discuss new insights into the origin of O VI absorbing gas that we have learned from combining the improved absorption-line measurements and highly complete galaxy survey data. The paper proceeds as follows: In Section 2 we present the full archival COS spectrum of PKS 0405–123 and new galaxy redshifts in our survey. In Section 3 we review measurements of the absorbers enabled by the COS spectrum including (1) a tentative detection of an O VI absorber at  $z = 0.2977$ , (2) a new O VI absorber at  $z = 0.3615$ , and (3) N V associated with a known O VI absorber at  $z = 0.3633$ . In Section 4 we discuss the galaxy environments of all seven O VI absorbers along this sightline and compare them to the galaxy environments of strong Ly $\alpha$  absorbers with no detected O VI. Finally, in Section 5, we briefly discuss the implications of our findings.

Throughout the paper, we adopt a  $\Lambda$  cosmology with  $\Omega_m = 0.3$ ,  $\Omega_\Lambda = 0.7$ , and  $H_0 = 70 \text{ km s}^{-1} \text{ Mpc}^{-1}$ . We also adopt a non-evolving, rest-frame absolute  $R$ -band magnitude (AB) of  $M_{R*} = -21.17$  for  $L_*$  galaxies based on Blanton et al. (2003). Unless otherwise stated, we perform  $k$ -corrections using the Scd galaxy template from Coleman et al. (1980).

## 2 DATA

PKS 0405–123 is a well-studied sightline with available imaging and UV spectroscopic data in the FUSE and HST archives (Chen & Prochaska 2000; Prochaska et al. 2004; Williger et al. 2006; Lehner et al. 2007). Different galaxy surveys have been carried out in this field identifying galaxies associated with absorption-line systems uncovered in the UV spectra (Spinrad et al. 1993; Ellingson & Yee 1994; Chen et al. 2005; Prochaska et al. 2006; Chen & Mulchaey 2009). Recently, PKS 0405–123 was targeted for HST/COS UV spectroscopy at significantly higher  $S/N$  than the archival STIS spectra. This new data set led to the

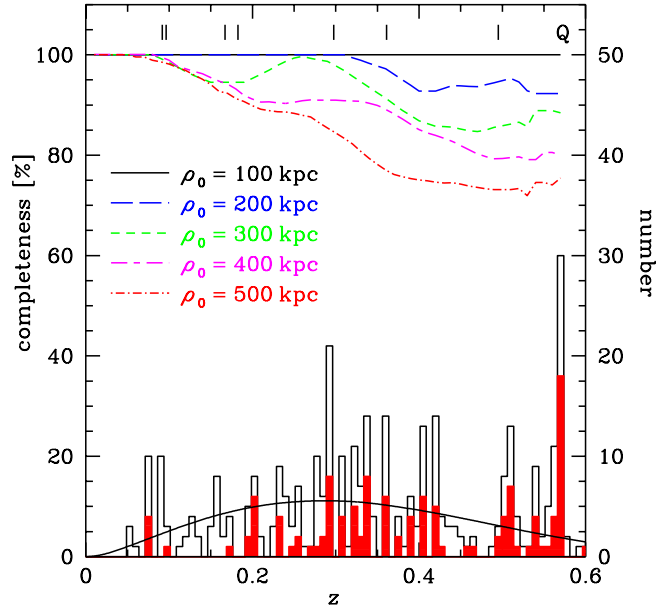


**Figure 2.** Summary of our galaxy survey results. The curves at the top show the estimated survey completeness for  $L > 0.1 L_*$  galaxies as a function of redshift at projected distances of  $\rho < 100$ , 200, 300, 400, and 500 kpc of the quasar sightline. The bottom histograms show the redshift distributions of all galaxies (black) and absorption-line dominated galaxies (red, solid) in the final combined spectroscopic catalog. For comparison, we show the expected redshift distribution based on a non-evolving  $R$ -band luminosity function adapted from Blanton et al. (2003), taking into account our survey incompleteness as a function of galaxy luminosity and redshift (solid black line). Spikes in the histogram that deviate significantly from expectations are due to large-scale galaxy overdensities in the quasar field. The redshifts of O VI absorbers (vertical ticks) and the quasar (Q) are shown along the top of the figure.

discovery of an interesting O VI absorber with no detectable H I at  $\Delta v \approx -300 \text{ km s}^{-1}$  from a previously detected O VI absorber in a partial Lyman-limit system at  $z = 0.1671$  (Savage et al. 2010). We have analyzed the full COS spectrum of PKS 0405–123 (Figure 1) together with new and existing galaxy survey data for a comprehensive study of the galactic environments of absorbing clouds uncovered along this quasar sightline.

### 2.1 COS spectroscopy

PKS 0405–123 was targeted for COS observations by two separate HST programmes (PI: Keith Noll, PID=11508 and PI: James Green, PID=11541). The two programs together acquired 17 exposures, totaling 22.2 ks with the G130M grating (covering the spectral range 1150 – 1450 Å and with full width at half-maximum spectral resolution of  $\text{FWHM} = 16 \text{ km s}^{-1}$ ), and 4 exposures, totaling 11.1 ks with the G160M grating (1400 – 1800 Å,  $\text{FWHM} = 16 \text{ km s}^{-1}$ ). The exposures were acquired at different central wavelengths in order to provide contiguous wavelength coverage despite the gap between COS detectors. We retrieved the 1-D individual calibrated spectra from the HST archive and combined them using a custom suite of software (see Yoon et al. 2012 for details). Specifically, individual spec-

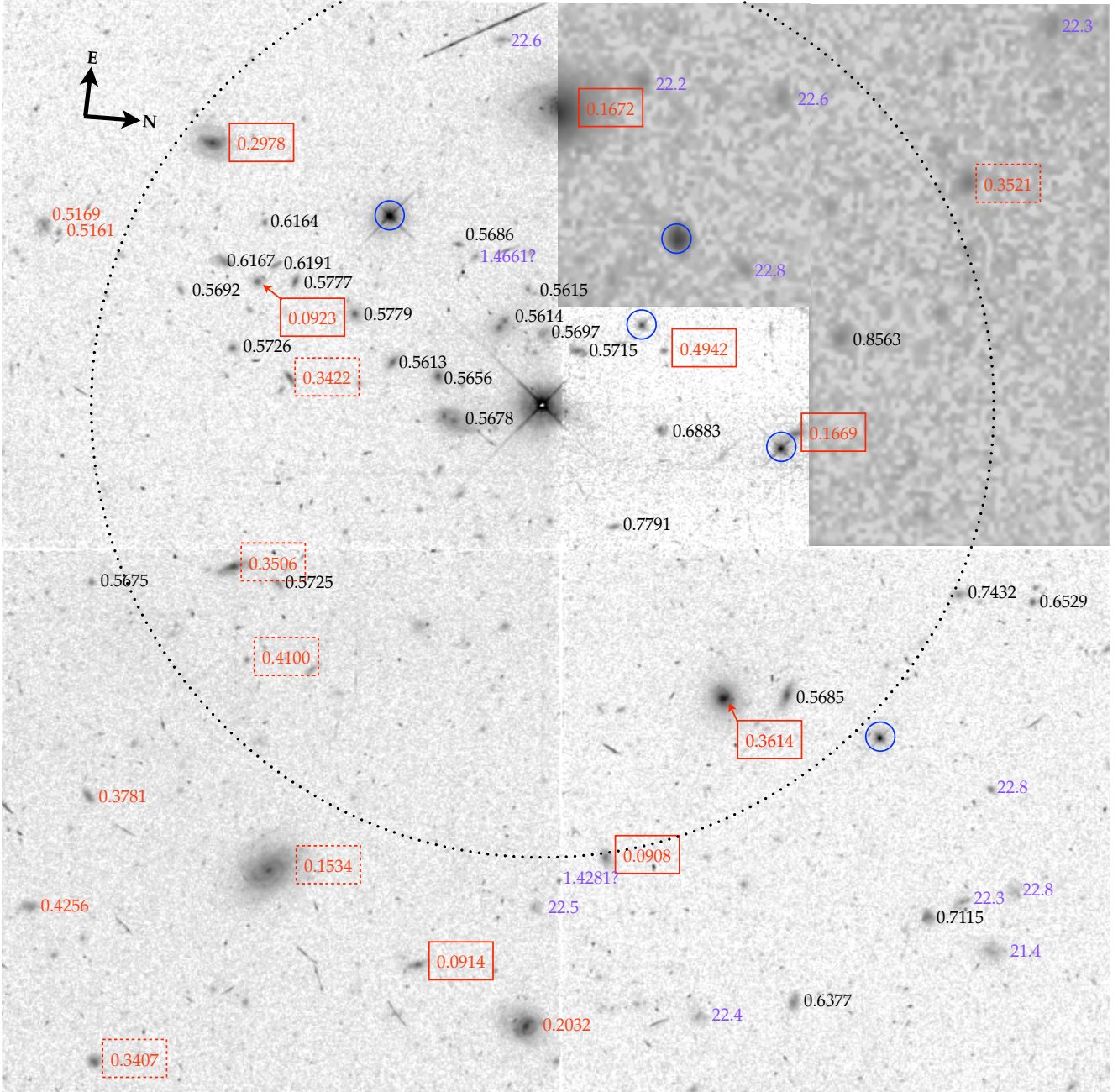


**Figure 3.** *HST*/Wide Field Planetary Camera 2 image of PKS 0405–123 augmented with an image from the DuPont telescope (Prochaska et al. 2006) where *HST* imagery is unavailable. The orientation of the field is indicated by the N–E arrows that appear in the upper-left corner. Redshifts are shown to the right of the corresponding galaxy except in crowded areas where an arrow is used to indicate association. Galaxies foreground to the quasar are shown in red, while background galaxies ( $z \gtrsim z_{\text{QSO}}$ ) are shown in black. Galaxies associated with OVI absorbers (with velocity offsets  $|\Delta v| < 300 \text{ km s}^{-1}$ ) are marked by solid red boxes, while galaxies associated with Ly $\alpha$  absorbers and no detectable OVI are marked by dotted red boxes. Stars are labelled with blue circles and galaxies without secure redshifts are marked in purple either by redshift (based on a single emission line) or *R*-band magnitude if no redshift is available. A dotted circle centered on the quasar with  $1'$  radius is shown to provide scale. In addition to the many foreground galaxies spectroscopically identified near the quasar line-of-sight, there exists a clear overdensity of galaxies at the redshift of the quasar.

tra from the two detector segments were aligned and co-added using a common Milky Way absorption line as a reference (e.g., Si III 1206) and then combined into a single one-dimensional spectrum. These co-addition routines work with photon counts rather than flux calibrated data to allow for an accurate error estimate in the low-count regime

(e.g. Gehrels 1986). A well-known issue with far-ultraviolet (FUV) spectra obtained using COS is the presence of fixed-pattern noise due to the grid-wire in the COS FUV detectors. Such pattern noise can be reduced by the use of multiple FP-POS settings (see the COS Instrument Handbook). As described above, PKS 0405–123 was observed by two dif-



**Table 1.** Journal of spectroscopic observations

Telescope	Instrument/setup	FWHM (Å)	No. of targets	Exposure time (ks)	Date
Magellan Baade	IMACS/f2/200l, 1'' slitlets	9	17	3.6	Nov. 2012
			12	3.0	Feb. 2011
			150	5.4	Nov. 2012
			140	5.4	Feb. 2011
Magellan Clay	LDSS3/VPH-all 1'' slitlets	10	24	7.2	Feb. 2011
APO 3.5-m	DIS/B400 & R300, 1.5'' long slit	5	23	varies	Oct.–Dec. 2012

ferent programs and in many exposures of different FP-POS settings. The effect of such fixed-pattern noise is therefore minimal in the final stack. To ensure consistency with previous results, we set a common zero-point by aligning the co-added COS spectrum with the archival FUSE and STIS spectra prior to combination of the G130M and G160M data. This alignment led to minor ( $\ll$ FWHM) higher-order corrections to the COS wavelength calibration. By comparing the COS spectrum with the archival STIS spectrum, we estimate that errors in the wavelength calibration limit the accuracy of line-centroids to  $\approx 4 \text{ km s}^{-1}$ .

The resulting high resolution spectrum (see Figure 1) enabled the new detections of O VI systems in addition to a number of other lines and significantly stronger upper limits on key ions. The new detections are discussed in detail in Section 3.

## 2.2 Galaxy Survey

Previous spectroscopic surveys of galaxies in the PKS 0405–123 field reached  $\approx 80\%$  completeness within a  $3'$  radius of the quasar sightline for galaxies brighter than  $R = 21$  and  $\approx 50\%$  for galaxies between  $R = 21$  and  $22$  (e.g. Chen & Mulchaey 2009). These surveys identified galaxies associated with half of the known O VI absorbers along this quasar sightline; however, a detailed study of the galaxy environments that includes sub- $L_*$  galaxies requires a higher survey completeness at fainter magnitudes. To improve the survey depth, we acquired new galaxy spectra with the Magellan telescopes using the Inamori-Magellan Areal Camera & Spectrograph (IMACS; Dressler et al. 2011) and the Low Dispersion Survey Spectrograph 3 (LDSS3) (see Table 1 for a summary of the observations). In addition, we confirmed a number of photometric stars using the Dual Imaging spectrograph (DIS) on the Apache Point 3.5-m. The IMACS and LDSS3 data were reduced using the Carnegie Observatories System for MultiObject Spectroscopy (COSMOS<sup>1</sup>) as described in Chen & Mulchaey (2009). The APO DIS spectra were reduced using a slightly modified version of the Low-REDUX pipeline written by J. Hennawi, S. Burles, and J. X. Prochaska<sup>2</sup>. Galaxy redshifts were determined both by cross-correlation with the Sloan Digital Sky Survey (SDSS; York et al. 2000) templates and by fitting of galaxy eigen-spectra as in Chen & Mulchaey (2009). In nearly all cases, the two independently determined redshifts were in good agreement ( $|\Delta z| \leq 0.0003$ ), but in the small number of

cases for which they were not, SDJ and HWC determined the best redshift by refitting and visual inspection. All assigned redshifts were visually inspected to determine their reliability and galaxy spectra were further classified as either absorption-line dominated or emission-line dominated. The final object catalog is presented in Table 2.

The new IMACS/LDSS3 observations include 225 new galaxies without previously known redshifts, providing an unprecedented level of completeness in the field when combined with previous surveys. Specifically, the survey is 100% ( $\approx 90\%$ ) complete for galaxies brighter than  $R = 22$  ( $R = 23$ ) within  $1'$  of the quasar sightline. The relevant figure-of-merit, however, is the completeness as a function of galaxy luminosity, physical impact parameter, and redshift which is shown in Figure 2 along with a galaxy-redshift histogram<sup>3</sup>. The survey is 100% complete for  $L > 0.1 L_*$  galaxies at impact parameters less than  $\rho = 100 \text{ kpc}$  and  $> 90\%$  complete at  $\rho < 200 \text{ kpc}$  at all redshifts  $z < z_{\text{QSO}}$ . The completeness level decreases somewhat at larger impact parameters due to our targeting priority, but even at  $\rho < 500 \text{ kpc}$ , the survey is  $\gtrsim 75\%$  complete for  $L > 0.1 L_*$  galaxies at  $z < z_{\text{QSO}}$ . The high level of completeness is visually captured by the *HST* image of the field labelled with galaxy redshifts (Figure 3).

We note that in addition to the many foreground galaxies spectroscopically identified near the quasar line-of-sight, there exists a clear overdensity of galaxies at the redshift of the quasar. The galaxy catalog is therefore also valuable for studying AGN fueling (e.g. Ellingson & Yee 1994).

## 3 NEW MEASUREMENTS OF ABSORPTION-LINE SYSTEMS

The higher  $S/N$  of the new COS data ensured both improved measurements of previously known transitions and new detections along the sightline. We conducted a systematic search of new absorption features in the COS spectra of PKS 0405–123 and identified three features that were previously unknown. These include: (1) a tentative detection of a new O VI absorber at  $z = 0.2977$ , (2) a new O VI component at  $\Delta v = +170 \text{ km s}^{-1}$  from a previously known metal-line absorber at  $z = 0.3608$ , and (3) NV absorption associated with a known O VI system at  $z = 0.3633$ . Combining previous results with the new findings yielded a sample of

<sup>1</sup> <http://code.obs.carnegiescience.edu/cosmos>

<sup>2</sup> <http://www.uchicago.edu/~xavier/LowRedux/>

<sup>3</sup> We estimated the completeness function using the observed completeness as a function of magnitude and angular separation from the quasar sightline and smoothed with a  $\Delta z = 0.1$  boxcar function to remove fluctuations due to small number statistics.

**Table 2.** The photometric and spectroscopic catalog of galaxies around PKS 0405–123<sup>a</sup>. The full table is available on the journal webpage.

ID	RA (J2000)	Dec (J2000)	$\Delta\theta$ ( $''$ )	$\rho^b$ (kpc)	$R$ (mag)	$z_{\text{spec}}$	Quality <sup>c</sup>	Object type <sup>d</sup>	Galaxy class <sup>e</sup>	$L/L_*^{b,f}$
80001 <sup>n</sup>	04:07:48.9	-12:11:33	7.8	35	$21.65 \pm 0.00$	0.5715	A	G	E	0.95
90001	04:07:49.1	-12:11:38	9.9	45	$22.10 \pm 9.99$	0.5697	A	G	E	0.62
80003 <sup>n</sup>	04:07:49.1	-12:11:43	11.7	53	$21.10 \pm 0.00$	0.5709	A	G	A	1.57
80004 <sup>n</sup>	04:07:48.2	-12:11:49	12.8	58	$19.97 \pm 0.00$	0.5678	A	G	A	4.36
80005 <sup>n</sup>	04:07:48.6	-12:11:52	15.5	70	$21.54 \pm 0.00$	0.5656	A	G	A	1.01
1883	04:07:48.3	-12:11:21	15.8	78	$21.69 \pm 0.12$	0.6883	A	G	E	1.69
90002	04:07:49.5	-12:11:41	16.3	74	$22.10 \pm 9.99$	0.5715	A	G	A	0.63
1920 <sup>n</sup>	04:07:47.4	-12:11:26	18.5	96	$22.77 \pm 0.19$	0.7797	A	G	A	0.97
1862	04:07:49.1	-12:11:21	18.5	78	$22.63 \pm 0.17$	0.4942	A	G	E	0.25
1866	04:07:48.8	-12:11:58	22.0	100	$21.40 \pm 0.10$	0.5713	A	G	E	1.19
80010 <sup>n</sup>	04:07:49.8	-12:11:48	23.1	-1	$21.70 \pm 0.00$	1.4657	B	G	E	-1.00
1820 <sup>n</sup>	04:07:49.9	-12:11:49	24.8	113	$21.75 \pm 0.13$	0.5686	A	G	A	0.85
1854	04:07:49.2	-12:12:04	29.6	136	$21.23 \pm 0.09$	0.5779	A	G	E	1.44

#### Notes

- <sup>a</sup> ID, coordinates, and  $R$ -band photometry from Prochaska et al. (2006) except for objects with IDs 800## or 900## which were added from Ellingson & Yee (1994) or based on visual inspection of the DuPont/WFCCD or *HST* images.  
<sup>b</sup> Given a value of  $-1$  when not available due to lack of a secure redshift or when not applicable.  
<sup>c</sup> Redshift and classification quality: A  $\rightarrow$  secure ( $\geq 2$  features), B  $\rightarrow$  1 feature, C  $\rightarrow$  observed but no features, N  $\rightarrow$  not observed.  
<sup>d</sup> Object classification: Q  $\rightarrow$  quasar, G  $\rightarrow$  galaxy, S  $\rightarrow$  star, U  $\rightarrow$  unknown.  
<sup>e</sup> Galaxy classification: E  $\rightarrow$  emission-line dominated, A  $\rightarrow$  absorption-line dominated, N  $\rightarrow$  n/a.  
<sup>f</sup> Measured from  $R$ -band photometry as discussed in text.  
<sup>n</sup> Redshift and classification from new data presented in this paper.

seven O VI absorbers and 12 individual components found at  $z = 0.0918\text{--}0.495$  along the sightline toward PKS 0405–123.

We measured the line profiles of both new and known O VI absorbers, as well as their associated H I and other metal transitions based on a Voigt profile analysis using the VPFIT package<sup>4</sup> (Carswell et al. 1987) and the empirical COS line spread function (LSF)<sup>5</sup>. The COS LSF exhibits broad wings which contain up to 40% of the flux (Ghavamian et al. 2009). The use of the empirical LSF in the Voigt profile fitting is therefore necessary in order to properly account for the absorption that falls in the wings of the LSF. In cases of line blending, we employed a simultaneous fit of a minimum number of separate components that are necessary to produce a reasonable  $\chi^2$  value. For non-detections, we calculated the  $3\text{-}\sigma$  rest-frame equivalent width limit over a  $300 \text{ km s}^{-1}$  spectral window (significantly broader than the wings of the COS LSF) and converted this to the corresponding  $3\text{-}\sigma$  limit in column density assuming that the gas is optically thin. The results are summarized in Table 3, where we list for each species the velocity offset  $\Delta v$  relative to the systemic redshift of each absorber  $z_{\text{sys}}$  as defined by the dominant H I component, the Doppler parameter  $b$ , and the best-fit column density. We also include in Table 3 measurements from the literature for completeness. Here we briefly describe the properties of newly detected absorption features.

At  $z = 0.1826$  and  $0.1829$ , two O VI components were found in previous searches (Prochaska et al. 2004; Thom & Chen 2008). We confirm both detections and remeasure the absorber properties with a simultaneous fit of both compo-

nents in the COS data. The lower-redshift O VI component is characterized by an O VI column density  $\log N(\text{O VI}) = 13.75 \pm 0.02$  and Doppler width  $b = 32 \pm 3 \text{ km s}^{-1}$ , and is merely  $\approx 9 \text{ km s}^{-1}$  offset from a previously identified H I absorption component with  $\log N(\text{H I}) = 14.69 \pm 0.01$  and  $b = 33 \pm 1 \text{ km s}^{-1}$ . The higher-redshift O VI component is characterized by  $\log N(\text{O VI}) = 13.88 \pm 0.02$  and  $b = 21 \pm 1 \text{ km s}^{-1}$ . No other ions have been detected with a  $3\text{-}\sigma$  upper limit of  $\log N < 12.8$  for both NV and Si IV absorption. Prochaska et al. (2004) reported an upper limit of  $\log N < 12.4$  for C III absorption. The best-fit Voigt profiles of the O VI doublet along with those of Ly $\alpha$  and Ly $\beta$  absorption are presented in the left column of Figure 4).

At  $z = 0.2977$ , we report a tentative detection of an O VI absorber at  $\Delta v \approx 8 \text{ km s}^{-1}$  from a previously identified Ly $\alpha$  absorber. The O VI absorption profile is relatively broad with  $\log N(\text{O VI}) = 13.61 \pm 0.02$  and  $b \approx 60 \text{ km s}^{-1}$ . The  $\lambda 1037$  member is detected at a  $\approx 7\text{-}\sigma$  level of significance, but the model slightly over-predicts the absorption strength of this weaker member which appears to be contaminated by other absorption features. No other metal absorption is detected in the COS spectrum. Our Voigt profile analysis shows that the Ly $\alpha$  transition is best described by two components separated by  $\Delta v = 65 \text{ km s}^{-1}$ , with one component containing  $\log N(\text{H I}) = 13.89 \pm 0.05$  at  $z = 0.2976$  and the other containing  $\log N(\text{H I}) = 13.34 \pm 0.2$  at  $z = 0.2979$ . The best-fit Voigt profiles of the O VI doublet along with those of Ly $\alpha$  and Ly $\beta$  absorption are presented in the middle-left column of Figure 4).

At  $z = 0.3615$ , we also report the detection of a new O VI component with  $\log N(\text{O VI}) = 13.80 \pm 0.01$  and  $b = 30 \pm 1 \text{ km s}^{-1}$  at  $\Delta v = +170 \text{ km s}^{-1}$  from a previously known absorption complex at  $z = 0.3608$  (e.g. Prochaska et al. 2004). Similar to the O VI absorber at  $z = 0.1829$ , we

<sup>4</sup> <http://www.ast.cam.ac.uk/~rfc/vpfit.html>

<sup>5</sup> [http://www.stsci.edu/hst/cos/performance/spectral\\_resolution/](http://www.stsci.edu/hst/cos/performance/spectral_resolution/)

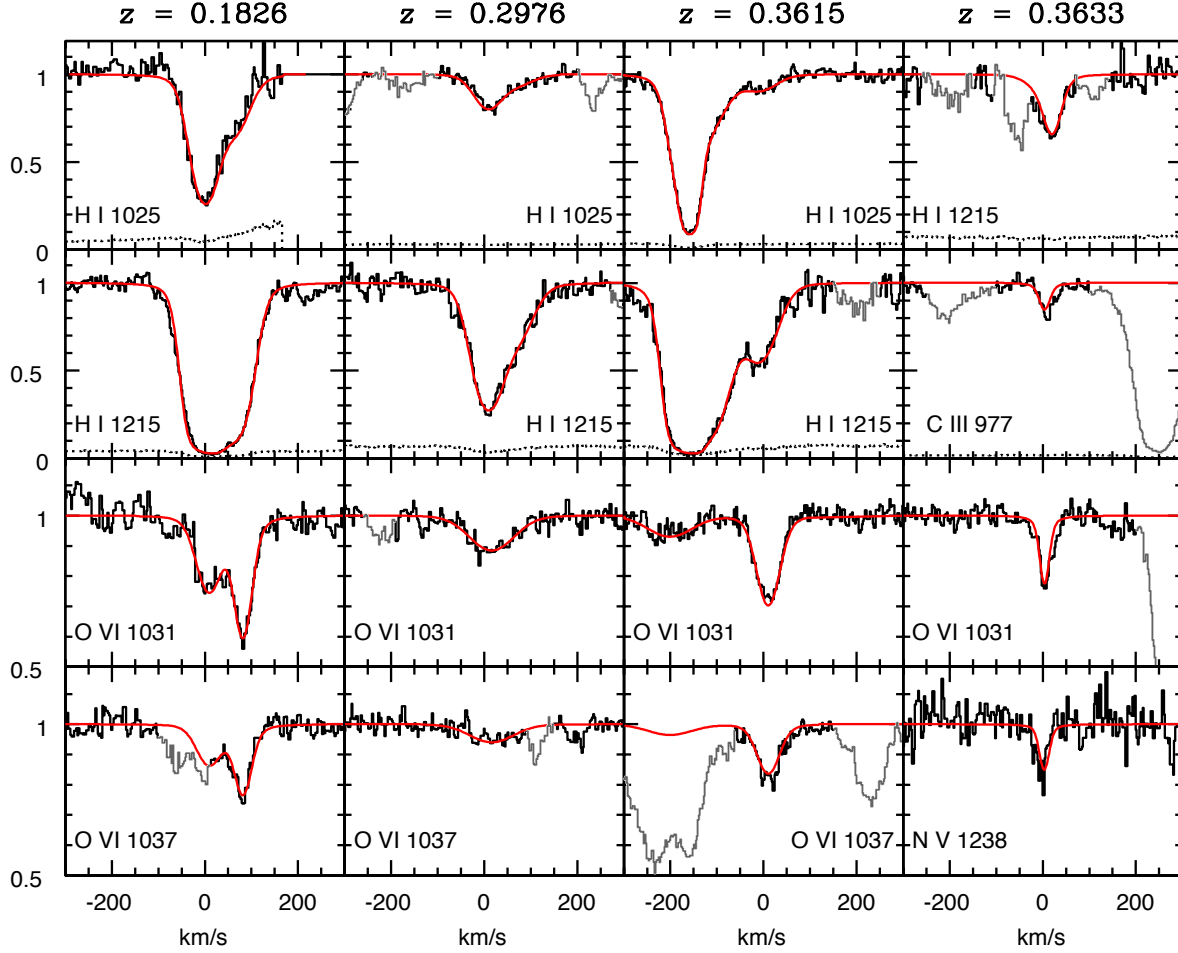


**Figure 4.** Absorption profiles of two O VI absorbers and a tentative detection (left three columns) and the NV doublet detected in a known metal-line absorber (right column) in the high-quality COS spectrum, along with the associated H I Ly $\alpha$  and/or Ly $\beta$  transition. The continuum normalized spectrum is shown in black solid line and the associated 1- $\sigma$  errors are plotted in black dotted line. The best-fit model profiles from a Voigt profile analysis (§ 3) are shown in red. Spectral regions contaminated by other absorption systems are plotted in gray. We do not plot data at velocities greater than  $\Delta v > +120 \text{ km s}^{-1}$  for the Ly $\beta$  line of the  $z = 0.1826$  absorber because in this range, the quasar flux is nearly completely attenuated by Milky Way Ly $\alpha$  absorption. We consider the O VI absorber at  $z = 0.2977$  a tentative detection, because the observed depth of the  $\lambda 1037$  member appears shallower than the expectation of the doublet based on the fit of the  $\lambda 1031$  member. Note that the bottom two rows are shown with a partial  $y$ -range from 0.5 to 1.2 to improve the visibility of weak features. This partial  $y$ -range prevents the errors from being displayed in the bottom two rows.

do not detect additional metal-line systems associated with this new O VI component. There is possible O VI absorption at  $z \approx 0.3608$  with  $\log N(\text{O VI}) = 13.38 \pm 0.05$  detected in the COS spectrum, but it cannot be confirmed due to contaminating features at the location of the second doublet member. The best-fit Voigt profiles of the O VI doublet along with those of Ly $\alpha$  and Ly $\beta$  absorption are presented in the middle-right column of Figure 4).

Finally, the O VI absorption system previously identified at  $z = 0.3633$  with  $\log N(\text{O VI}) = 13.36 \pm 0.05$  and  $b = 10 \pm 1 \text{ km s}^{-1}$  displays possible presence of associated NV doublet in the new COS spectrum. Prochaska et al. (2004) identified H I, O IV, N IV, and C III absorption associated with this O VI absorber, although the H I absorbing component is  $\Delta v = +20 \text{ km s}^{-1}$  away from the O VI absorber. We confirm the presence of C III absorption with  $\log N(\text{C III}) = 12.48 \pm 0.07$  and detect NV with  $N(\text{NV}) = 13.01 \pm 0.08$  at the redshift of the O VI absorber.

The measurements were obtained based on a simultaneous fit of Voigt profiles to all three transitions, assuming that these ions originate in the same gas. Allowing independent fits to the line centroids of NV and C III does not improve the model-fit. The best-fit Voigt profiles of Ly $\alpha$ , C III  $\lambda 977$ , O VI  $\lambda 1031$  and NV  $\lambda 1238$  are presented in the right column of Figure 4). Both  $\text{O}^{5+}$  and  $\text{N}^{4+}$  are highly ionized species, whereas  $\text{C}^{2+}$  is at a much lower ionization state. The presence of these ions together strongly support a photo-ionization scenario for the absorbing gas (see Prochaska et al. 2004). Based on the observed relative abundance of  $\text{C}^{2+}$  and  $\text{O}^{5+}$ , Prochaska et al. 2004 derived an ionization parameter of  $\log U = -1.4 \pm 0.2$  and a minimum metallicity of solar for the absorbing gas assuming that all of the observed  $N(\text{H I})$  is associated with the O VI absorbing gas.

Including the tentative detection of an O VI absorber at  $z = 0.2977$ , we have a total of seven O VI absorbers along the sightline toward PKS 0405–123. In addition, this sight-

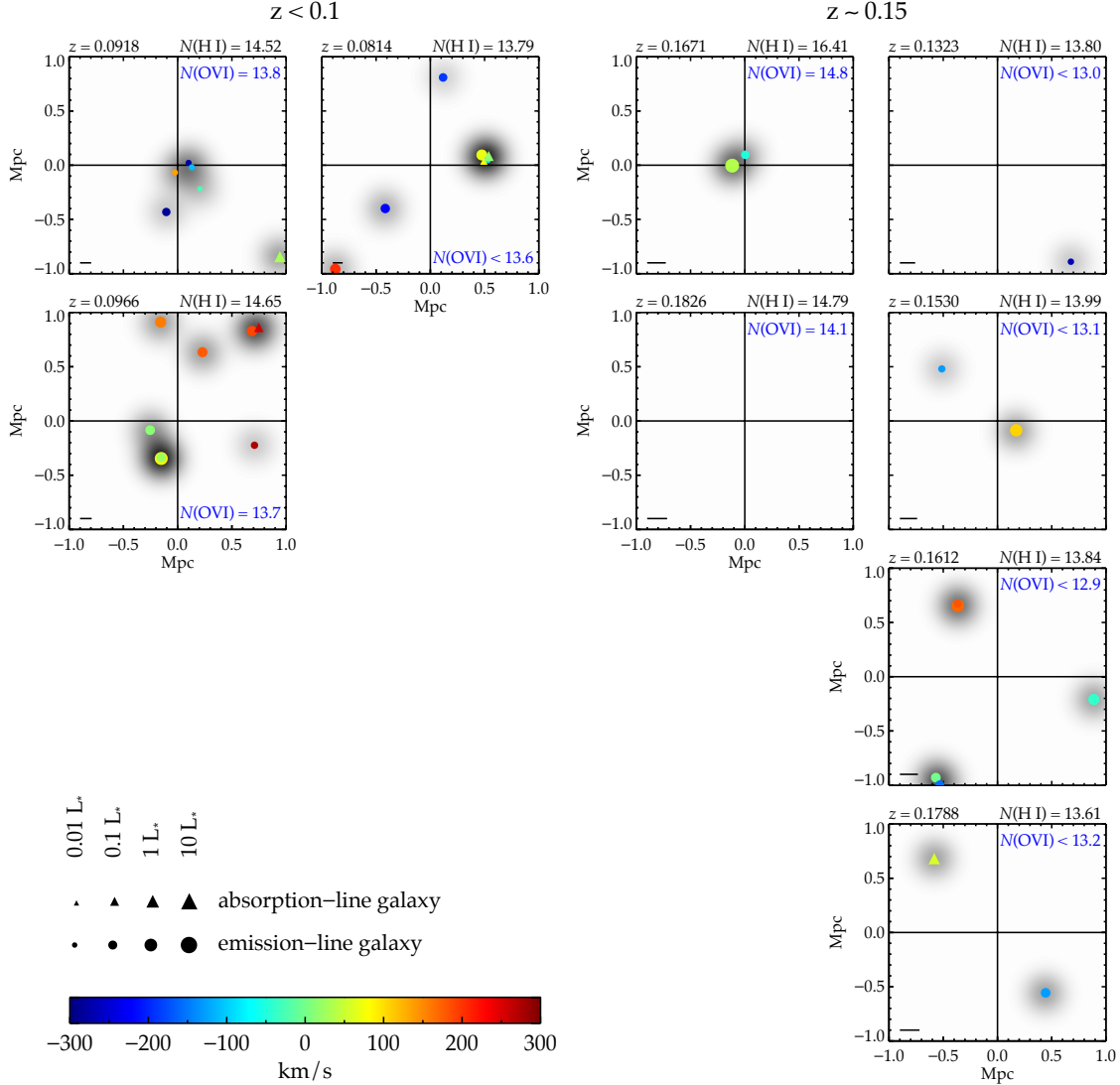


**Figure 5.** The galaxy environments of O VI absorbers and strong Ly $\alpha$  absorbers of  $\log N(\text{H I}) > 13.6$  with no detectable O VI (designated as “Ly $\alpha$ -only” systems). Considering the increasing survey incompleteness of faint ( $< 0.1 L_*$ ) galaxies with increasing redshift, we separate the galaxy-absorber sample into four redshift bins. For each redshift bin, we show the spatial and velocity distributions of galaxies around O VI absorbers in the left column and Ly $\alpha$ -only absorbers in the right column. Each panel is centered at the quasar, while positions of galaxies with projected line-of-sight velocity  $|\Delta v| < 300 \text{ km s}^{-1}$  of the absorber are marked with circles for emission-line galaxies and triangles for absorption-line galaxies. The symbols are color-coded to indicate the line-of-sight velocity between each galaxy and the absorber. The symbol size specifies galaxy luminosity as shown in the figure legend. To help visualize the surface density of surrounding galaxies, we also introduce a gray-scale showing a luminosity-weighted galaxy surface density where each galaxy is represented by a Gaussian with FWHM = 300 kpc. The luminosity weighting assigns  $L \geq L_*$  galaxies a peak of 1,  $0.1 \leq L < L_*$  galaxies a peak of 0.7 and  $L < 0.1 L_*$  galaxies a peak of 0.4.

line contains additional 11 strong Ly $\alpha$  absorption systems of  $\log N(\text{H I}) > 13.6$  (Williger et al. 2006; Lehner et al. 2007)<sup>6</sup> with no detectable absorption from heavy ions. The high  $S/N$  of the COS spectrum enables stronger limits (cf. Prochaska et al. 2004) on the associated O VI column den-

ties. We define a subsample of “Ly $\alpha$ -only” absorbers of these strong Ly $\alpha$  absorbers with no associated O VI absorption to a sensitive upper limit. The properties of these Ly $\alpha$ -only systems are summarized in Table 4.

#### 4 THE GALAXY ENVIRONMENTS OF O VI AND Ly $\alpha$ -ONLY ABSORBER

The highly complete survey data of faint galaxies in the field around PKS 0405–123 offer a new opportunity to re-examine the galaxy environments of O VI absorbers. In particular, we compare our findings with previous results from a

<sup>6</sup> We associate the HI components identified by Lehner et al. (2007) with one another provided  $|\Delta v| < 300 \text{ km s}^{-1}$ . Lehner et al. (2007) restricted their study to absorbers with  $z < 0.5$  so we include systems identified by Williger et al. (2006) at  $z > 0.5$  as well. For each system, we adopt the total HI column density and the redshift of the strongest HI component.



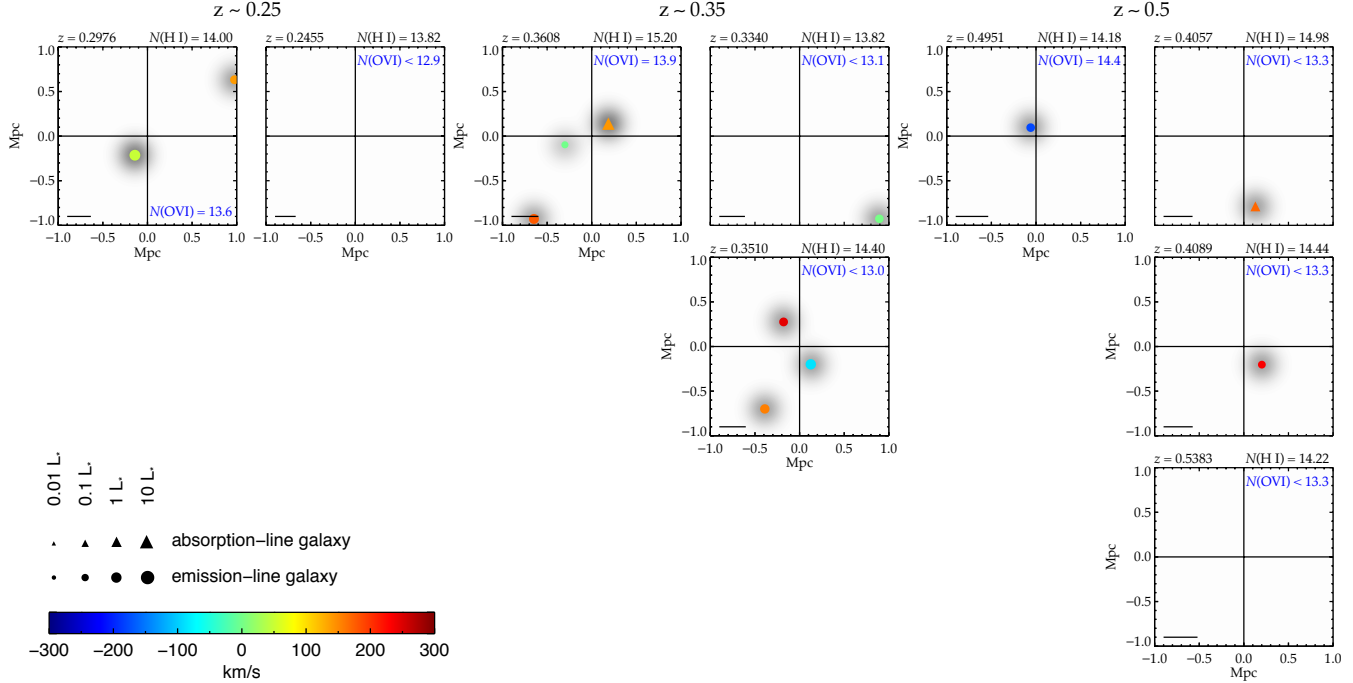


Figure 5. continued

shallower survey which concluded that O VI absorbers trace a diverse set of environments including: the halos of individual galaxies, galaxy groups, filamentary-like structures, and galaxy voids (e.g. Prochaska et al. 2006). In addition, we compare the galaxy environments of the O VI absorbers with those of Ly $\alpha$ -only absorbers which constitutes a control sample in seeking the discriminating galactic features that result in the observed O VI absorbing gas at large galactic radii. Throughout, we associate galaxies with absorbers provided the projected line-of-sight velocity between the absorber and the galaxy is  $|\Delta v| < 300 \text{ km s}^{-1}$ . All galaxies spectroscopically identified at impact parameter  $\rho < 1 \text{ Mpc}$  and velocity offset  $|\Delta v| < 300 \text{ km s}^{-1}$  of the O VI and Ly $\alpha$ -only systems are presented in Tables 5 and 6, respectively.

The galactic environments of O VI absorbers uncovered in our survey are presented in Figure 5. We find that O VI primarily traces over-dense galaxy environments with at least one emission-line galaxy found within  $\rho \approx 300 \text{ kpc}$ . Specifically, the O VI absorber at  $z = 0.0918$  was originally attributed to filamentary structure connecting three galaxy groups at  $\rho = 1 - 3 \text{ Mpc}$  (Prochaska et al. 2006). However, we have uncovered four dwarf, emission-line galaxies at  $\rho \leq 300 \text{ kpc}$ , the closest of which is at  $\rho = 70 \text{ kpc}$  and  $\Delta v = +140 \text{ km s}^{-1}$ . Similarly, the absorbers at  $z \approx 0.3608$  had been attributed to the intragroup medium of a group of passive galaxies found at  $\rho = 1 - 3 \text{ Mpc}$ . Our survey has revealed a dwarf emission-line galaxy ( $L = 0.08 L_*$  at  $\rho = 320 \text{ kpc}$  and  $\Delta v \approx 0 \text{ km s}^{-1}$ ) in addition to the known massive absorption-line galaxy previously found at  $\rho = 230 \text{ kpc}$ . The only intriguing exception is the O VI absorption system at  $z \approx 0.183$ , which exhibits two strong components separated by  $70 \text{ km s}^{-1}$ . This O VI absorber does not have an associated galaxy at  $\rho < 300 \text{ kpc}$ . Our galaxy survey rules out the presence of any galaxies of  $L > 0.04 L_*$  at  $\rho < 250 \text{ kpc}$  and the presence of any galaxies of  $L > 0.3 L_*$  at  $\rho < 1 \text{ Mpc}$ .

The lack of galaxies found in the vicinity suggests that this metal-enriched absorber resides in an apparent void. Finally, the O VI absorber at  $z = 0.495$  with associated Ne VIII doublet (Narayanan et al. 2011) is found to be associated with an emission-line galaxy at  $\rho = 110 \text{ kpc}$  (Chen & Mulchaey 2009). Our new survey has not uncovered any additional galaxies in the vicinity of the absorber. We are able to rule out the presence of any galaxies with  $L > 0.1 L_*$  at  $\rho < 200 \text{ kpc}$ .

We also present in Figure 5 the galaxy environments of O VI and Ly $\alpha$ -only absorbers. Considering the increasing survey incompleteness of faint ( $< 0.1 L_*$ ) galaxies with increasing redshift, we separate the galaxy-absorber sample into four redshift bins. For each redshift bin, we show the spatial and velocity distributions of galaxies around O VI absorbers in the left column and Ly $\alpha$ -only absorbers in the right column. Each panel is centered at the quasar, while galaxy positions are marked with circles for emission-line galaxies and triangles for absorption-line galaxies. The symbols are color-coded to indicate the line-of-sight velocity between each galaxy and the absorber. The symbol size specifies galaxy luminosity as shown in the figure legend. To help visualize the surface density of surrounding galaxies, we also introduce a gray-scale showing luminosity-weighted galaxy surface density where each galaxy is represented by a Gaussian with FWHM =  $300 \text{ kpc}$ .

A qualitative finding based on Figure 5 is that a larger fraction of Ly $\alpha$ -only absorbers appear in underdense or relatively isolated galaxy environments in comparison to those of O VI absorbers. Considering all the absorbers together, six of the seven O VI absorption systems at  $z < 0.5$  along the sightline are associated with at least one galaxy with  $\rho \lesssim 300 \text{ kpc}$ . Four of the six O VI absorption systems at  $z < 0.4$  are found in a group of multiple galaxies with  $\rho \lesssim 300 \text{ kpc}$ . In

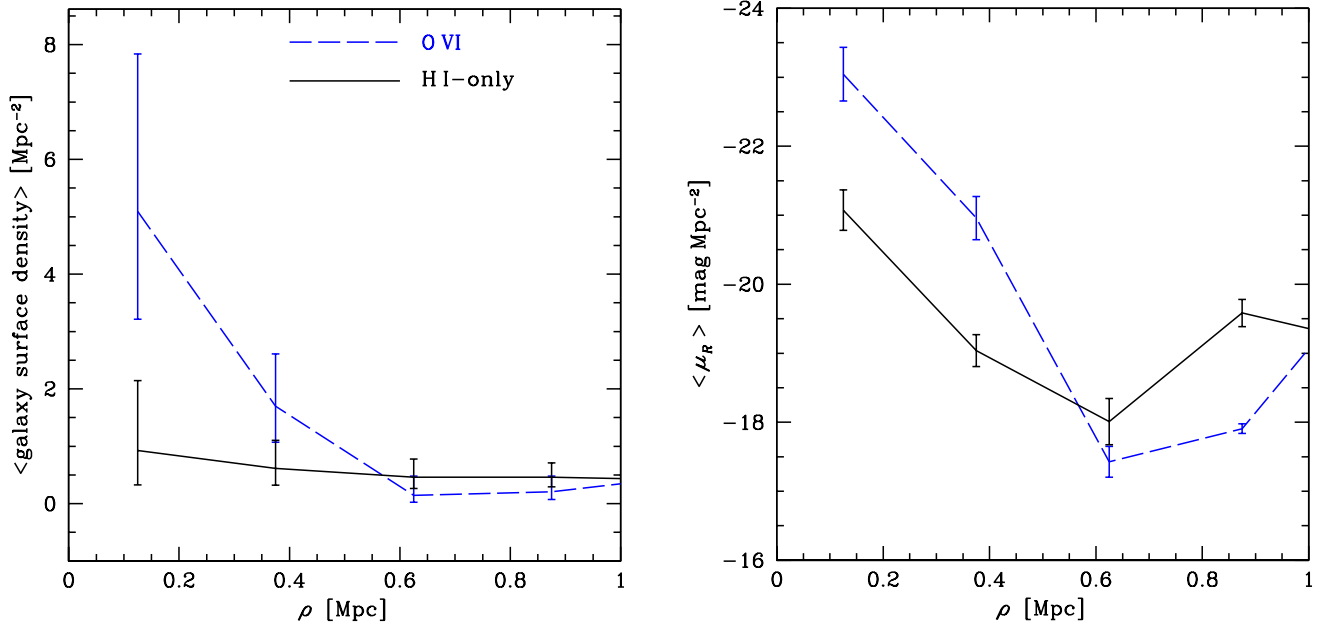


**Figure 6.** Mean radial profiles of the galaxy distribution around O VI and Ly $\alpha$ -only absorbers. The *left* panel shows the mean surface density of galaxies versus projected distance around O VI (dashed line) and Ly $\alpha$ -only (solid line) absorbers, and the *right* panel shows the mean surface brightness profiles. Galaxy density error-bars are computed from Poisson confidence intervals while surface brightness uncertainties are computed using a jackknife resampling technique to indicate uncertainties due to sample variance. It is clear that there exists an overdensity of galaxies within  $\rho \approx 500$  kpc radius of O VI absorbers, which is not seen around Ly $\alpha$ -only absorbers. Similarly, the mean galaxy surface brightness profile around O VI absorbers exhibits a steep rise by  $\Delta\mu_R \approx +5 \text{ mag Mpc}^{-2}$  toward the inner regions at  $\rho \lesssim 500$  kpc, while the galaxy surface brightness profile around Ly $\alpha$ -only absorbers remains comparatively flat with  $\Delta\mu_R \approx +2 \text{ mag Mpc}^{-2}$ .

contrast, of the 11 additional Ly $\alpha$ -only absorbers, only three have associated galaxies found at  $\rho < 300$  kpc.

To quantify the potential difference in the observed galactic environments between O VI and Ly $\alpha$ -only absorbers, we perform two separate tests in the following discussion. First, we examine the mean radial profiles of galaxy properties averaged over all systems in each subsample. Second, we examine the distribution of galaxy properties within each subsample. In both tests, the comparisons are based on both the surface density of the galaxies and the surface brightness of star light.

#### 4.1 Do O VI and Ly $\alpha$ -only absorbers share similar azimuthally averaged galaxy distributions out to 1 Mpc?

To determine whether or not O VI and Ly $\alpha$ -only absorbers occur in similar galaxy environments, we measure the mean radial profile of the galaxy distribution around these absorbers by first stacking the observed 2D distribution of galaxies around individual absorbers shown in Figure 5 and then computing an azimuthal average in annuli with increasing radius. The left panel of Figure 6 displays the mean galaxy surface density profiles around O VI absorbers (dashed line) and Ly $\alpha$ -only absorbers (solid line). Error-bars show our estimate of uncertainties due to counting statistics (e.g. Gehrels 1986). It is clear that there exists an overdensity of galaxies within a  $\rho \approx 500$  kpc radius of O VI absorbers, which is not seen around Ly $\alpha$ -only absorbers.

Such distinction between O VI and Ly $\alpha$ -only absorbers

is also seen in the observed mean surface brightness profiles around these absorbers (the right panel of Figure 6). In this case, error-bars are computed using a jackknife resampling technique to estimate uncertainties due to sample variance. While the mean galaxy surface brightness profile around O VI absorbers exhibits a steep rise of  $\Delta\mu_R \approx +5 \text{ mag Mpc}^{-2}$  toward the inner regions at  $\rho \lesssim 500$  kpc, only a mild increase of  $\Delta\mu_R \approx +2 \text{ mag Mpc}^{-2}$  is seen in the galaxy surface brightness profile around Ly $\alpha$ -only absorbers.

#### 4.2 Do O VI and Ly $\alpha$ -only absorbers share similar galaxy distribution functions in the inner 500 kpc?

The exercise presented in § 4.1 shows that the ensemble average of the radial profiles of galaxy surface density and surface brightness exhibit different characteristics at  $\rho \lesssim 500$  kpc between O VI and Ly $\alpha$ -only absorbers. Here we focus on the inner regions of  $\rho = 500$  kpc radius around individual absorbers and examine whether there is a difference in the variation of galaxy properties within each subsample. This exercise provides further insights into the immediate galactic environments of individual absorbers.

The left panel of Figure 7 shows the cumulative fraction of absorbers originating in environments of no more than  $N_{\text{gal}}$  galaxies. It shows that while 16% of O VI absorbers occur in environments where no galaxies are found within a radius of  $\rho = 500$  kpc, more than 50% of Ly $\alpha$ -only absorbers occur in such “voids”. However, the samples are small and a Kolmogorov-Smirnov (KS) test shows that the probabil-

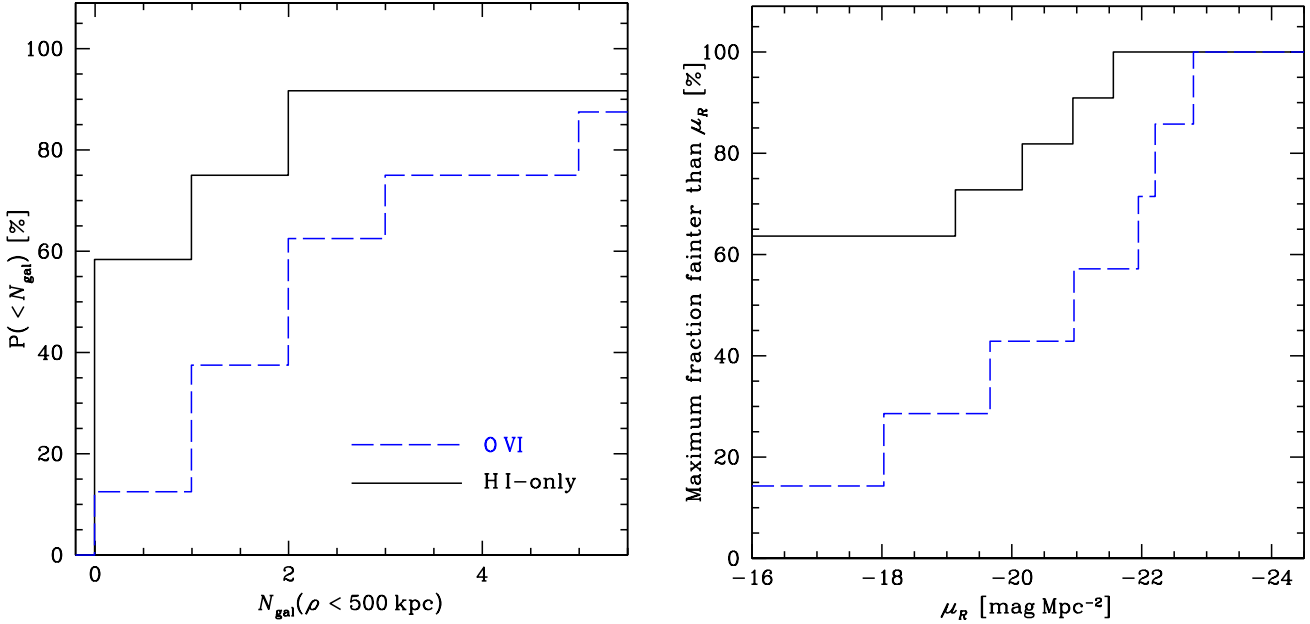


**Figure 7.** Cumulative fraction of absorbers originating in environments with no more than  $N_{\text{gal}}$  galaxies within a radius of  $\rho = 500$  kpc (*left panel*) and with mean surface brightness (averaged over the area of 500 kpc radius) fainter than rest-frame  $R$ -band magnitude  $\mu_R$  per square Mpc (*right panel*). While a larger fraction of Ly $\alpha$ -only absorbers ( $> 50\%$  versus  $16\%$  for O VI absorbers) arise in environments where no luminous galaxies are found within a radius of  $\rho = 500$  kpc, no statistically significant distinction can be made between the cumulative fraction of galaxy surface density around O VI and Ly $\alpha$ -only absorbers based on these small samples. Specifically, a Kolmogorov-Smirnov (KS) test on their cumulative distribution functions shows that the probability that O VI and Ly $\alpha$ -only absorbers are drawn from a similar parent galaxy environment distributions is at most  $20\%$  (galaxy density) and  $8\%$  (surface brightness).

ity that both types of absorbers are drawn from a similar underlying environment distribution is  $20\%$ .

Next, we examine the mean surface density of star light averaged over the area within 500 kpc radius in units of rest-frame  $R$ -band magnitude per square Mpc. This quantity allows us to account for missing galaxies that are too faint to be detected in our survey by including the survey limit in our analysis. Including non-detections, the right panel of Figure 7 shows the maximum possible cumulative fraction of absorbers arising in environments with mean galaxy surface brightness fainter than the designated value  $\mu_R$ . Similar to the surface density plot in the left panel, we find that as much as  $60\%$  of Ly $\alpha$ -only absorbers originate in environments with galaxy surface brightness fainter than  $\mu_R \approx -19 \text{ mag Mpc}^{-2}$ , while no more than  $35\%$  of O VI absorbers are found in such low surface brightness environments. A KS test shows that there is at most  $8\%$  probability that O VI and Ly $\alpha$ -only absorbers trace the same underlying galaxy population.

## 5 DISCUSSION AND CONCLUSIONS

The high level of completeness achieved at faint magnitudes by our survey has allowed us to probe the galaxy populations to low luminosities and obtain better understanding of the nature of the absorbing systems. We have shown that O VI absorbers previously attributed to a gaseous medium connecting massive galaxy groups are, in fact, more closely associated with less massive groups containing at least one dwarf, emission-line galaxy. In total, four of seven known O VI absorbers along the PKS 0405–123 sightline reside in

galaxy “groups” that contain at least one star-forming member. Two of the seven are found nearby to an emission-line galaxy and only one O VI absorber is found in a galaxy void. Therefore, we conclude that O VI absorbers primarily trace gas-rich environments as indicated by the presence of at least one low-mass, emission-line galaxy seen in our survey. However, the presence of  $\text{O}^{5+}$  ions could either be the result of starburst driven outflows or due to stripped material from galaxy interactions that also trigger star formation.

This is in stark contrast to lower ionization transitions such as Mg II that are found to reside primarily in the halos of isolated galaxies both with and without star formation (Steidel et al. 1997). One exception is those ultra-strong Mg II absorbers with rest-frame absorption equivalent width  $W_r(2796) > 3 \text{ \AA}$ . Three of these ultra-strong Mg II systems have been targeted for follow-up galaxy surveys and all three are found in groups containing multiple super- $L_*$  galaxies (e.g. Whiting et al. 2006; Nestor et al. 2011; Gauthier 2013), with an inferred group halo mass of  $M_h \sim 10^{13} M_\odot$ . The galaxy “groups” found around O VI absorbers in our survey contain primarily low-luminosity (and presumably low-mass) galaxies (see also Mulchaey & Chen 2009), and are therefore not as massive as those found near ultra-strong Mg II absorbers. A detailed comparison of the dynamics between galaxies and absorbing gas may lead to further insights into the physical origin of these O VI absorbers.

In addition, our analysis reveals a clear distinction in the radial profiles of mean galaxy surface density and surface brightness around different absorbers. Specifically, O VI absorbers are found to reside in galaxy overdensities with significantly higher mean galaxy surface density and surface

**Table 3.** Summary of line properties of known O VI absorbers

Element	$\Delta v$ (km s <sup>-1</sup> )	$b$ (km s <sup>-1</sup> )	$\log N / \text{cm}^{-2}$	References <sup>a</sup>
$z_{\text{sys}} = 0.09180$				
HI	0	$38 \pm 2$	$14.52 \pm 0.05$	1
C IV	0		$< 12.90$	2
N V	0		$< 12.67$	2
O VI	+20		$13.83 \pm 0.04$	1
Si IV	0		$< 12.66$	2
$z_{\text{sys}} = 0.09658$				
HI	0	$40 \pm 2$	$14.65 \pm 0.05$	1
C IV	0		$< 12.90$	2
N V	0		$< 12.97$	2
O VI	0		$13.70 \pm 0.20$	1
Si IV	0		$< 12.64$	2
$z_{\text{sys}} = 0.16711$				
HI	$-11 \pm 3$		15.50	1, 3
HI	$0 \pm 5$		16.35	1, 3
O VI	$-266 \pm 5$	$52 \pm 2$	$13.90 \pm 0.03$	3
O VI	$-35 \pm 2$		$14.71 \pm 0.01$	3
$z_{\text{sys}} = 0.18259$				
HI	$0 \pm 4$	$33 \pm 1$	$14.69 \pm 0.01$	2
HI	$+68 \pm 4$	$36 \pm 2$	$14.09 \pm 0.03$	2
N V	0		$< 12.83$	2
O VI	$+9 \pm 4$	$32 \pm 3$	$13.75 \pm 0.02$	2
O VI	$+82 \pm 4$	$21 \pm 1$	$13.88 \pm 0.02$	2
Si IV	0		$< 12.77$	2
$z_{\text{sys}} = 0.29762$				
HI	$0 \pm 5$	$38 \pm 3$	$13.89 \pm 0.05$	2
HI	$+65 \pm 15$	$42 \pm 12$	$13.34 \pm 0.19$	2
C III	0		$< 12.05$	2
N V	0		$< 13.13$	2
O VI <sup>b</sup>	$+8 \pm 4$	$63 \pm 4$	$13.61 \pm 0.02$	2
$z_{\text{sys}} = 0.36078$				
HI	$-24 \pm 14$	$26 \pm 8$	$14.3 \pm 0.3$	2
HI	$0 \pm 3$	$16 \pm 1$	$15.06 \pm 0.05$	2
HI	$+27 \pm 8$	$54 \pm 6$	$14.29 \pm 0.08$	2
HI	$+151 \pm 4$	$45 \pm 4$	$13.56 \pm 0.04$	2
HI <sup>c</sup>	$+557 \pm 3$	$41 \pm 10$	$12.75 \pm 0.41$	2
HI	$+575 \pm 3$	$22 \pm 5$	$13.11 \pm 0.14$	2
C III	+168		$< 12.5$	2
C III <sup>c</sup>	$+557 \pm 3$	12	$12.48 \pm 0.07$	2
N V	+168		$< 13.1$	2
N V <sup>c</sup>	$+557 \pm 3$	11	$13.01 \pm 0.08$	2
O VI <sup>b</sup>	$-44 \pm 7$	$64 \pm 9$	$13.38 \pm 0.05$	2
O VI	$+168 \pm 3$	$30 \pm 1$	$13.80 \pm 0.01$	2
O VI <sup>c</sup>	$+557 \pm 3$	10	$13.36 \pm 0.05$	2
$z_{\text{sys}} = 0.49510$				
HI	0	$53 \pm 1$	$14.09 \pm 0.03$	4
HI	+93	$21 \pm 2$	$13.44 \pm 0.09$	4
O VI	-3	$35 \pm 1$	$14.29 \pm 0.02$	4
O VI	+48	$19 \pm 2$	$13.80 \pm 0.07$	4

<sup>a</sup> 1: Prochaska et al. 2004; 2: this work;

3: Savage et al. 2010; 4: Narayanan et al. 2011.

<sup>b</sup> Tentative detection due to contamination of the  $\lambda 1037$  member.<sup>c</sup> Measurements obtained with a simultaneous fit to the transitions assuming that these absorbers originate in the same gas.**Table 4.** Summary of line properties of strong Ly $\alpha$  absorbers with no detectable O VI absorption

Element	$\Delta v$ (km s <sup>-1</sup> )	$b$ (km s <sup>-1</sup> )	$\log N / \text{cm}^{-2}$	References <sup>a</sup>
$z_{\text{sys}} = 0.08139$				
HI	0	$54 \pm 4$	$13.79 \pm 0.02$	1
O VI	0		$< 13.62$	2
$z_{\text{sys}} = 0.13233$				
HI	0	$22 \pm 2$	$13.64 \pm 0.03$	1
HI	+193	$32 \pm 6$	$13.29 \pm 0.06$	1
C IV	0		$< 12.94$	3
N V	0		$< 12.97$	3
O VI	0		$< 12.95$	3
Si IV	0		$< 12.83$	3
$z_{\text{sys}} = 0.15304$				
HI	-208	$22 \pm 2$	$13.54 \pm 0.04$	1
HI	0	$46 \pm 3$	$13.80 \pm 0.03$	1
C IV	0		$< 13.30$	3
N V	0		$< 12.71$	3
O VI	0		$< 13.14$	3
Si IV	0		$< 12.56$	3
$z_{\text{sys}} = 0.16121$				
HI	0	$54 \pm 8$	$13.71 \pm 0.04$	1
HI	+75	$18 \pm 4$	$13.27 \pm 0.09$	1
N V	0		$< 13.11$	3
O VI	0		$< 12.85$	3
Si IV	0		$< 12.42$	3
$z_{\text{sys}} = 0.17876$				
HI	0	$55 \pm 7$	$13.61 \pm 0.04$	1
C III	0		$< 12.37$	3
N V	0		$< 13.13$	3
O VI	0		$< 13.16$	3
$z_{\text{sys}} = 0.24554$				
HI	-99	$54 \pm 24$	$13.23 \pm 0.11$	1
HI	0	$23 \pm 2$	$13.69 \pm 0.03$	1
O VI	0		$< 12.89$	3
Si IV	0		$< 12.53$	3
$z_{\text{sys}} = 0.33402$				
HI	0	$30 \pm 2$	$13.82 \pm 0.03$	1
N V	0		$< 13.04$	3
O VI	0		$< 13.12$	3
$z_{\text{sys}} = 0.35099$				
HI	0	$38 \pm 2$	$14.25 \pm 0.03$	1
HI	+115	$25 \pm 5$	$13.53 \pm 0.05$	1
HI	+251	$31 \pm 5$	$13.57 \pm 0.05$	1
C III	0		$< 12.14$	3
N V	0		$< 13.05$	3
O VI	0		$< 13.00$	3
$z_{\text{sys}} = 0.40571$				
HI	0	$33 \pm 2$	$14.98 \pm 0.02$	1
C III	0		$< 12.00$	3
N V	0		$< 13.10$	3
O VI	0		$< 13.28$	3

<sup>a</sup> 1: Lehner et al. 2007; 2: from FUSE data published in Prochaska et al. 2004; 3: this work; 4: Williger et al. 2006

**Table 4.** Continued.

Element	$\Delta v$ (km s <sup>-1</sup> )	$b$ (km s <sup>-1</sup> )	$\log N / \text{cm}^{-2}$	References <sup>a</sup>
$z_{\text{sys}} = 0.40886$				
HI	0	$40 \pm 2$	$14.38 \pm 0.03$	1
HI	+149	$26 \pm 6$	$13.58 \pm 0.07$	1
N V	0		$< 13.12$	3
O VI	0		$< 13.28$	3
$z_{\text{sys}} = 0.53830$				
HI	0	$23 \pm 4$	$14.22 \pm 0.06$	4
C III	0		$< 12.35$	3
O VI	0		$< 13.26$	3

<sup>a</sup> 1: Lehner et al. 2007; 2: from FUSE data published in Prochaska et al. 2004; 3: this work; 4: Williger et al. 2006

brightness at  $\rho \lesssim 500$  kpc, while only a mild increase in galaxy surface brightness is seen at small  $\rho$  around strong Ly $\alpha$ -only absorbers.

On the other hand, Chen & Mulchaey (2009) showed that both strong Ly $\alpha$  absorbers of  $\log N(\text{HI}) \geq 14$  and O VI absorbers exhibit a comparable clustering amplitude as emission-line dominated galaxies. The apparent discrepancy between the finding of this paper and those of Chen & Mulchaey (2009) may be explained by the intrinsic difference in the sample definition. Our current study is based on galaxies and absorbers found in a single field, and therefore limited by the small sample size. In particular, we have defined a controlled Ly $\alpha$ -only sample that includes Ly $\alpha$  absorbers that are as weak as  $\log N(\text{HI}) \approx 13.6$  in order to have a sufficiently large sample for a statistical analysis. In contrast, the O VI absorbers in the comparison sample all have associated Ly $\alpha$  with  $\log N(\text{HI}) > 14$ . It is therefore unclear whether the observed distinction between the galactic environments of O VI and Ly $\alpha$ -only absorbers represents a fundamental difference between metal and HI absorbers, or between high and low HI column density clouds. We expect that such uncertainty in the interpretation of the observations will be resolved with a larger sample of galaxy and absorber data from different fields complemented by multi-band imaging data. Together, these data will help constrain galaxy star-formation rates and reveal the presence of any faint tidal features (e.g. Chen & Mulchaey 2009).

Lastly, an intriguing outcome of our deep galaxy survey is the discovery of an O VI absorber that is likely to reside in a “void”. This O VI absorption system at  $z \approx 0.183$ , which exhibits two strong components separated by  $70 \text{ km s}^{-1}$ , does not have other ionic transitions detected to sensitive limits (Table 3; see also Prochaska et al. 2004). Our galaxy survey data rule out the presence of any galaxies of  $L > 0.04 L_*$  at  $\rho < 250$  kpc or the presence of any galaxies of  $L > 0.3 L_*$  at  $\rho < 1$  Mpc. The lack of additional ionic transitions associated with this absorber suggests that the gas may be hot and collisionally ionized. Also, the lack of galaxies found in the vicinity suggests that this absorber resides in an apparent void, similar to an O VI absorber at  $z=0.06807$  for which Tripp et al. (2006) ruled out the presence of galaxies of  $L > 0.04 L_*$  at  $\rho < 200$  kpc. While a likely explanation for the origin of the gas is the warm-hot inter-

galactic medium, it is unclear whether the relatively narrow line width is consistent with a diffuse intergalactic origin.

## ACKNOWLEDGEMENTS

It is a pleasure to thank Jean-René Gauthier and the anonymous referee for helpful comments that significantly improved the manuscript. We thank Edward Villanueva and Daniel Kelson for their help with the COSMOS reduction pipeline and Joe Hennawi for his aid with the Low-Redux reduction pipeline. We made extensive use of the XIDL library provided by Jason Prochaska. We are grateful for the support provided by the staff at the Las Campanas Observatory and the Apache Point Observatory. SDJ acknowledges funding from a National Science Foundation Graduate Research Fellowship and a fellowship from the Illinois Space Grant Consortium. This research has made use of the NASA Astrophysics Data System and the NASA/IPAC Extragalactic Database (NED) which is operated by the Jet Propulsion Laboratory, California Institute of Technology, under contract with the National Aeronautics and Space Administration. This paper contains data obtained with the 6.5-m Magellan Telescopes located at Las Campanas Observatory, Chile and data obtained with the Apache Point Observatory 3.5-meter telescope, which is owned and operated by the Astrophysical Research Consortium.

## REFERENCES

- Blanton M. R., Hogg D. W., Bahcall N. A., Brinkmann J., Britton M., Connolly A. J., Csabai I., Fukugita M., Loveday J., Meiksin A., Munn J. A., Nichol R. C., Okamura S., Quinn T., Schneider D. P., Shimasaku K., Strauss M. A., ... Weinberg D. H., 2003, *ApJ*, 592, 819
- Burles S., Tytler D., 1996, *ApJ*, 460, 584
- Carswell R. F., Webb J. K., Baldwin J. A., Atwood B., 1987, *ApJ*, 319, 709
- Cen R., 2012, *ApJ*, 753, 17
- Cen R., Ostriker J. P., 1999, *ApJ*, 514, 1
- Chen H.-W., Mulchaey J. S., 2009, *ApJ*, 701, 1219
- Chen H.-W., Prochaska J. X., 2000, *ApJL*, 543, L9
- Chen H.-W., Prochaska J. X., Weiner B. J., Mulchaey J. S., Williger G. M., 2005, *ApJL*, 629, L25
- Coleman G. D., Wu C.-C., Weedman D. W., 1980, *ApJS*, 43, 393
- Danforth C. W., Shull J. M., 2008, *ApJ*, 679, 194
- Dressler A., Bigelow B., Hare T., Sutin B., Thompson I., Burley G., Epps H., Oemler A., Bagish A., Birk C., Clardy K., Gunnels S., Kelson D., Shethman S., Osip D., 2011, *PASP*, 123, 288
- Ellingson E., Yee H. K. C., 1994, *ApJS*, 92, 33
- Gauthier J.-R., 2013, *MNRAS*, 432, 1444
- Gehrels N., 1986, *ApJ*, 303, 336
- Ghavamian P., Aloisi A., Lennon D., Hartig G., Kriss G. A., Oliveira C., Massa D., Keyes T., Proffitt C., Delker T., Osterman S., 2009, Technical report, Preliminary Characterization of the Post-Launch Line Spread Function of COS
- Green J. C., Froning C. S., Osterman S., Ebbets D., Heap S. H., Leitherer C., Linsky J. L., Savage B. D., Sembach



- K., Shull J. M., Siegmund O. H. W., Snow T. P., Spencer J., Stern S. A., Stocke J., Welsh B., B  land S., Burgh E. B., Danforth C., 2012, *ApJ*, 744, 60
- Howk J. C., Ribaldo J. S., Lehner N., Prochaska J. X., Chen H.-W., 2009, *MNRAS*, 396, 1875
- Kang H., Ryu D., Cen R., Song D., 2005, *ApJ*, 620, 21
- Lehner N., Savage B. D., Richter P., Sembach K. R., Tripp T. M., Wakker B. P., 2007, *ApJ*, 658, 680
- Moos H. W., Cash W. C., et al. 2000, *ApJL*, 538, L1
- Mulchaey J. S., Chen H.-W., 2009, *ApJL*, 698, L46
- Mulchaey J. S., Davis D. S., Mushotzky R. F., Burstein D., 1996, *ApJ*, 456, 80
- Narayanan A., Savage B. D., Wakker B. P., Danforth C. W., Yao Y., Keeney B. A., Shull J. M., Sembach K. R., Froning C. S., Green J. C., 2011, *ApJ*, 730, 15
- Nestor D. B., Johnson B. D., Wild V., M  nard B., Turnshek D. A., Rao S., Pettini M., 2011, *MNRAS*, 412, 1559
- Oppenheimer B. D., Dav   R., 2006, *MNRAS*, 373, 1265
- Oppenheimer B. D., Dav   R., 2009, *MNRAS*, 395, 1875
- Oppenheimer B. D., Dav   R., Katz N., Kollmeier J. A., Weinberg D. H., 2012, *MNRAS*, 420, 829
- Prochaska J. X., Chen H.-W., Howk J. C., Weiner B. J., Mulchaey J., 2004, *ApJ*, 617, 718
- Prochaska J. X., Weiner B., Chen H.-W., Cooksey K. L., Mulchaey J. S., 2011, *ApJS*, 193, 28
- Prochaska J. X., Weiner B. J., Chen H.-W., Mulchaey J. S., 2006, *ApJ*, 643, 680
- Richter P., Savage B. D., Tripp T. M., Sembach K. R., 2004, *ApJS*, 153, 165
- Savage B. D., Narayanan A., Wakker B. P., Stocke J. T., Keeney B. A., Shull J. M., Sembach K. R., Yao Y., Green J. C., 2010, *ApJ*, 719, 1526
- Smith B. D., Hallman E. J., Shull J. M., O’Shea B. W., 2011, *ApJ*, 731, 6
- Spinrad H., Filippenko A. V., Yee H. K., Ellingson E., Blades J. C., Bahcall J. N., Jannuzi B. T., Bechtold J., Dobrzycki A., 1993, *AJ*, 106, 1
- Steidel C. C., Dickinson M., Meyer D. M., Adelberger K. L., Sembach K. R., 1997, *ApJ*, 480, 568
- Stinson G. S., Brook C., Prochaska J. X., Hennawi J., Shen S., Wadsley J., Pontzen A., Couchman H. M. P., Quinn T., Macci   A. V., Gibson B. K., 2012, *MNRAS*, 425, 1270
- Stocke J. T., Keeney B. A., Danforth C. W., Shull J. M., Froning C. S., Green J. C., Penton S. V., Savage B. D., 2013, *ApJ*, 763, 148
- Stocke J. T., Penton S. V., Danforth C. W., Shull J. M., Tumlinson J., McLin K. M., 2006, *ApJ*, 641, 217
- Tepper-Garc  a T., Richter P., Schaye J., Booth C. M., Dalla Vecchia C., Theuns T., Wiersma R. P. C., 2011, *MNRAS*, 413, 190
- Thom C., Chen H.-W., 2008, *ApJ*, 683, 22
- Tilton E. M., Danforth C. W., Shull J. M., Ross T. L., Ross T. L., 2012, *ApJ*, 759, 112
- Tripp T. M., Aracil B., Bowen D. V., Jenkins E. B., 2006, *ApJL*, 643, L77
- Tripp T. M., Savage B. D., 2000, *ApJ*, 542, 42
- Tripp T. M., Savage B. D., Jenkins E. B., 2000, *ApJL*, 534, L1
- Tripp T. M., Sembach K. R., Bowen D. V., Savage B. D., Jenkins E. B., Lehner N., Richter P., 2008, *ApJS*, 177, 39
- Tumlinson J., Thom C., Werk J. K., Prochaska J. X., Tripp T. M., Weinberg D. H., Peebles M. S., O’Meara J. M., Oppenheimer B. D., Meiring J. D., Katz N. S., Dav   R., Ford A. B., Sembach K. R., 2011, *Science*, 334, 948
- Wakker B. P., Savage B. D., 2009, *ApJS*, 182, 378
- Whiting M. T., Webster R. L., Francis P. J., 2006, *MNRAS*, 368, 341
- Williger G. M., Heap S. R., Weymann R. J., Dav   R., Ellingson E., Carswell R. F., Tripp T. M., Jenkins E. B., 2006, *ApJ*, 636, 631
- Woodgate, B. E., et al. 1998, *PASP*, 110, 1183
- Yoon J. H., Putman M. E., Thom C., Chen H.-W., Bryan G. L., 2012, *ApJ*, 754, 84
- York D. G., Adelman J., Anderson Jr. J. E., et al. 2000, *AJ*, 120, 1579

This paper has been typeset from a  $\text{\LaTeX}$  file prepared by the author.

**Table 5.** Summary of spectroscopically identified galaxies at  $\rho < 1$  Mpc and  $|\Delta v| < 300$  km s $^{-1}$  of O VI absorbers

ID	R.A. (J2000)	Decl. (J2000)	$\Delta\alpha$ ( $''$ )	$\Delta\delta$ ( $''$ )	$\Delta\theta$ ( $''$ )	$\rho$ (kpc)	R (mag)	$z_{\text{spec}}$	galaxy class <sup>a</sup>	$L/L_*$
$z_{\text{sys}} = 0.09180$ $\log N(\text{HI}) = 14.52$ $\log N(\text{O VI}) = 13.83$ $N_{\text{gal}} = 5$										
1835	04:07:49.4	-12:12:16	14.2	-39.3	41.8	71	$21.31 \pm 0.10$	0.0923	E	0.02
2055	04:07:44.4	-12:11:24	-59.1	12.7	60.4	102	$21.30 \pm 0.09$	0.0908	E	0.02
2080	04:07:43.2	-12:11:48	-76.7	-11.3	77.5	132	$21.27 \pm 0.09$	0.0914	E	0.02
2212	04:07:40.2	-12:13:44	-120.7	-127.3	175.4	299	$21.94 \pm 0.13$	0.0917	E	0.01
1698	04:07:52.6	-12:15:49	61.1	-252.3	259.6	439	$19.74 \pm 0.07$	0.0908	E	0.07
$z_{\text{sys}} = 0.09658$ $\log N(\text{HI}) = 14.65$ $\log N(\text{O VI}) = 13.70$ $N_{\text{gal}} = 5$										
1457	04:07:58.1	-12:12:24	141.8	-47.3	149.5	267	$19.03 \pm 0.07$	0.0966	E	0.15
1602	04:07:54.2	-12:14:45	84.6	-188.3	206.5	370	$19.01 \pm 0.07$	0.0967	E	0.15
1601	04:07:54.2	-12:14:50	84.6	-193.3	211.0	379	$16.74 \pm 0.06$	0.0969	E	1.24
2254	04:07:39.7	-12:05:42	-128.0	354.7	377.1	679	$18.74 \pm 0.07$	0.0973	E	0.20
1659	04:07:54.4	-12:03:07	87.5	509.7	517.1	931	$17.99 \pm 0.06$	0.0972	E	0.39
$z_{\text{sys}} = 0.16711$ $\log N(\text{HI}) = 16.41$ $\log N(\text{O VI}) = 14.77$ $N_{\text{gal}} = 2$										
80006	04:07:48.3	-12:11:03	-1.9	33.7	33.7	96	$21.04 \pm 0.00$	0.1669	E	0.08
1753	04:07:51.2	-12:11:38	40.6	-1.3	40.6	116	$17.43 \pm 0.06$	0.1672	E	2.13
$z_{\text{sys}} = 0.18259$ $\log N(\text{HI}) = 14.79$ $\log N(\text{O VI}) = 14.12$ $N_{\text{gal}} = 0$										
no galaxies of $L > 0.04 L_*$ at $\rho < 250$ kpc and no galaxies of $L > 0.3 L_*$ at $\rho < 1$ Mpc										
$z_{\text{sys}} = 0.29762$ $\log N(\text{HI}) = 14.00$ $\log N(\text{O VI}) = 13.61$ $N_{\text{gal}} = 1$										
1786	04:07:50.6	-12:12:25	31.8	-48.3	57.9	256	$19.34 \pm 0.07$	0.2978	E	1.38
$z_{\text{sys}} = 0.36078$ $\log N(\text{HI}) = 15.20$ $\log N(\text{O VI}) = 13.94$ $N_{\text{gal}} = 2$										
1967	04:07:45.9	-12:11:09	-37.1	27.7	46.3	233	$18.58 \pm 0.07$	0.3614	A	4.47
1716	04:07:52.5	-12:11:56	59.7	-19.3	62.7	316	$23.01 \pm 0.21$	0.3608	E	0.08
$z_{\text{sys}} = 0.49510$ $\log N(\text{HI}) = 14.18$ $\log N(\text{O VI}) = 14.41$ $N_{\text{gal}} = 1$										
1862	04:07:49.1	-12:11:21	9.8	15.7	18.5	112	$22.63 \pm 0.17$	0.4942	E	0.25

<sup>a</sup> galaxy classification: E→ emission-line dominated, A→ absorption-line dominated.

**Table 6.** Summary of spectroscopically identified galaxies at  $\rho < 1$  Mpc and  $|\Delta v| < 300 \text{ km s}^{-1}$  of Ly $\alpha$ -only absorbers

ID	R.A. (J2000)	Decl. (J2000)	$\Delta\alpha$ (")	$\Delta\delta$ (")	$\Delta\theta$ (")	$\rho$ (kpc)	R (mag)	$z_{\text{spec}}$	galaxy class <sup>a</sup>	$L/L_*$
$z_{\text{sys}} = 0.08139$ $\log N(\text{H I}) = 13.79$ $\log N(\text{O VI}) < 13.62$ $N_{\text{gal}} = 6$										
2757	04:07:27.3	-12:10:35	-309.8	61.7	315.9	486	$17.70 \pm 0.06$	0.0817	E	0.35
2804	04:07:26.5	-12:11:12	-321.5	24.7	322.5	496	$20.11 \pm 0.07$	0.0817	A	0.04
2860	04:07:24.9	-12:11:03	-345.0	33.7	346.6	530	$20.40 \pm 0.08$	0.0811	E	0.03
2867	04:07:24.5	-12:10:41	-350.9	55.7	355.2	545	$18.35 \pm 0.07$	0.0815	A	0.19
1117	04:08:06.9	-12:15:57	270.8	-260.3	375.6	571	$18.81 \pm 0.07$	0.0806	E	0.12
2110	04:07:43.2	-12:02:49	-76.7	527.7	533.2	812	$19.36 \pm 0.07$	0.0807	E	0.07
$z_{\text{sys}} = 0.13233$ $\log N(\text{H I}) = 13.80$ $\log N(\text{O VI}) < 12.95$ $N_{\text{gal}} = 0$										
no galaxies of $L > 0.1 L_*$ at $\rho < 250$ kpc and no galaxies of $L > 0.16 L_*$ at $\rho < 1$ Mpc										
$z_{\text{sys}} = 0.15304$ $\log N(\text{H I}) = 13.99$ $\log N(\text{O VI}) < 13.14$ $N_{\text{gal}} = 2$										
2034	04:07:44.0	-12:12:09	-65.0	-32.3	72.6	193	$18.24 \pm 0.07$	0.1534	E	0.84
1334	04:08:01.6	-12:08:36	193.1	180.7	264.4	701	$21.75 \pm 0.13$	0.1525	E	0.03
$z_{\text{sys}} = 0.16121$ $\log N(\text{H I}) = 13.84$ $\log N(\text{O VI}) < 12.85$ $N_{\text{gal}} = 3$										
1503	04:07:57.4	-12:07:41	131.5	235.7	269.9	752	$18.19 \pm 0.07$	0.1619	E	0.99
1504	04:07:57.5	-12:07:34	133.0	242.7	276.7	771	$21.45 \pm 0.11$	0.1619	E	0.05
2784	04:07:26.6	-12:12:52	-320.1	-75.3	328.8	912	$19.08 \pm 0.07$	0.1611	E	0.43
$z_{\text{sys}} = 0.17876$ $\log N(\text{H I}) = 13.61$ $\log N(\text{O VI}) < 13.16$ $N_{\text{gal}} = 2$										
2282	04:07:38.4	-12:14:41	-147.1	-184.3	235.8	711	$20.46 \pm 0.08$	0.1783	E	0.15
1345	04:08:01.6	-12:07:51	193.1	225.7	297.0	898	$19.25 \pm 0.07$	0.1790	A	0.46
$z_{\text{sys}} = 0.24554$ $\log N(\text{H I}) = 13.82$ $\log N(\text{O VI}) < 12.89$ $N_{\text{gal}} = 0$										
no galaxies of $L > 0.07 L_*$ at $\rho < 250$ kpc and no galaxies of $L > 0.5 L_*$ at $\rho < 1$ Mpc										
$z_{\text{sys}} = 0.33402$ $\log N(\text{H I}) = 13.82$ $\log N(\text{O VI}) < 13.12$ $N_{\text{gal}} = 0$										
no galaxies of $L > 0.13 L_*$ at $\rho < 250$ kpc and no galaxies of $L > 0.5 L_*$ at $\rho < 1$ Mpc										
$z_{\text{sys}} = 0.35099$ $\log N(\text{H I}) = 14.40$ $\log N(\text{O VI}) < 13.00$ $N_{\text{gal}} = 3$										
1939	04:07:46.7	-12:12:17	-25.4	-40.3	47.7	235	$20.18 \pm 0.08$	0.3506	E	0.95
1787	04:07:50.9	-12:10:41	36.2	55.7	66.4	329	$21.48 \pm 0.11$	0.3521	E	0.29
1652	04:07:53.8	-12:13:58	78.7	-141.3	161.8	802	$20.95 \pm 0.09$	0.3517	E	0.47
$z_{\text{sys}} = 0.40571$ $\log N(\text{H I}) = 14.98$ $\log N(\text{O VI}) < 13.28$ $N_{\text{gal}} = 1$										
80008	04:07:46.8	-12:14:02	-23.9	-145.3	147.3	800	$20.93 \pm 0.00$	0.4065	A	0.69
$z_{\text{sys}} = 0.40886$ $\log N(\text{H I}) = 14.44$ $\log N(\text{O VI}) < 13.28$ $N_{\text{gal}} = 1$										
1975	04:07:45.9	-12:12:14	-37.1	-37.3	52.6	287	$22.70 \pm 0.21$	0.4100	E	0.14
$z_{\text{sys}} = 0.53830$ $\log N(\text{H I}) = 14.22$ $\log N(\text{O VI}) < 13.26$ $N_{\text{gal}} = 0$										
no galaxies of $L > 0.5 L_*$ at $\rho < 250$ kpc and no galaxies of $L > 0.5 L_*$ at $\rho < 1$ Mpc										

<sup>a</sup> galaxy classification: E→ emission-line dominated, A→ absorption-line dominated.